HAL open science

Specific trends in phosphate glass crystallization

Jean Rocherullé, M. Cai, Patricia Benard-Rocherulle, J. Troles, J. Massera, L. Petit, Ronan Lebullenger, Laurent Calvez, Xianghua Zhang, David Le Coq

To cite this version:

Jean Rocherullé, M. Cai, Patricia Benard-Rocherulle, J. Troles, J. Massera, et al.. Specific trends in phosphate glass crystallization. Journal of Non-Crystalline Solids, 2021, 551, pp.120431. 10.1016/j.jnoncrysol.2020.120431 . hal-03003216

HAL Id: hal-03003216

https://hal.science/hal-03003216v1

Submitted on 17 Oct 2022

HAL is a multi-disciplinary open access archive for the deposit and dissemination of scientific research documents, whether they are published or not. The documents may come from teaching and research institutions in France or abroad, or from public or private research centers.

L'archive ouverte pluridisciplinaire **HAL**, est destinée au dépôt et à la diffusion de documents scientifiques de niveau recherche, publiés ou non, émanant des établissements d'enseignement et de recherche français ou étrangers, des laboratoires publics ou privés.

Distributed under a Creative Commons Attribution - NonCommercial 4.0 International License

Version of Record: https://www.sciencedirect.com/science/article/pii/S0022309320305433
Manuscript_f15edb0117e05b8bca2f210fc103295c

Specific trends in phosphate glass crystallization

J. Rocherullé, Muzhi Cai, P. Bénard-Rocherullé, R. Lebullenger, L. Calvez, J. Trolès, D. Le Coq, X-H Zhang

J. Massera*, L. Petit*

Glass and Ceramic group, ISCR, UMR CNRS 6226, University of Rennes, 35042 Rennes (France)

* Tampere University, Faculty of Medicine and Health Technology, Tampere (Finland)

Abstract

This paper focusses on investigating and comparing the congruent crystallization of phosphate glasses with different degrees of polymerization. The study was performed both on powders, with different size fractions, and coarse particles which can be assimilated to bulk. From DSC experiments, corroborated by SEM analysis, it was demonstrated that $LiPO_3$ crystallizes from surface whereas $LiGe_2(PO_4)_3$ crystallizes in the whole volume. $Sn_2P_2O_7$ presented both phenomena, the nucleation time lag being short enough to observe internal crystallization at the laboratory time scale. Using the non-isothermal Ozawa method, the kinetic parameters of the overall devitrification process were determined in terms of the Avrami exponent and of the activation energy for crystallization.

The temperature of the maximum nucleation rate was calculated by using the nucleation adiabatic theory. For the achievement of this calculation, the heat capacity temperature dependence up to melting was determined from DSC experiments. The results were found in a good agreement with the SEM observation and the results of the non-isothermal crystallization study.

© 2020 published by Elsevier. This manuscript is made available under the CC BY NC user license
https://creativecommons.org/licenses/by-nc/4.0/

1. Introduction

Over the years and according to Scopus database, the number of publications dealing with phosphate glasses were of about 10 per year from 1950 till the beginning of the 70's. Then, it has increased exponentially since these last 4 decades. Indeed, for a long time, the low chemical resistance of phosphate glasses, compared to ordinary silicate, led to reluctance in studying/using such glass family. However, with time, the unique properties of phosphate glasses has led to an increasing interest by the scientific community.

The most well-known property that differentiates phosphate glasses, from others glass families, is their low melting temperatures, which makes the melting of phosphates less energy and time consuming. Nevertheless, their preparation requires the use of crucible materials other than platinum-based, due to the corrosion that phosphate batches usually cause.

Among all the applications, one can mention bioactive glasses [1] and laser host materials [2] for which phosphates have made unusual achievements. As an example, they have been investigated as bioresorbable materials for targeted tissue repair applications. Their tunable properties, in terms of ion release rates and cytocompatibility [3], are controlled by varying their chemical compositions. In addition, their coefficient of thermal expansion being very high, they have been also used to seal low temperature components [4]. The study of lithium bearing phosphate glasses with relatively high, electrical conductivity has also been very prolific because of their potential applications as solid electrolytes for secondary batteries and by the fact they can be compatible with most of the electrode materials in use [5]. In the same way, phosphate-based glass-ceramics, for which the crystallizing phases are related to the NASICON structural type, have among the highest electrical conductivity of all solid electrolytes to date [6].

The other characteristic that has make phosphate glasses attractive is the degree of flexibility of their networks that allows for the solubility of very high amounts of heavy metal oxides without any phase separation or devitrification phenomena that could deteriorate their

properties. Besides, when containing high amounts of iron oxides, the chemical durability is considerably increased up to values better than those of silicates [7].

All these properties of phosphate glasses have always been closely related to their network structure, as in other glass systems. There is no doubt that NMR is a particularly powerful method to investigate the structure of phosphate glasses, facilitated by the high relative sensitivity of the ^{31}P nucleus as compared to ^{29}Si.

It is well known that the network of phosphate glasses is built up of PO_4 units, for which, at least one of the oxygens forms a non-branching point with neighboring tetrahedral.

In any case, the interpretation of the structure in phosphate glasses always follows the same rule than the one used in the case of silicate and borosilicate glasses by taking into account the number of bridging oxygens per tetrahedron (Q^n).

If the solid state NMR of ^{31}P nuclei constitutes the most common way of approaching the structure of phosphate glasses, the Raman and FTIR spectroscopies have been those mostly used. These two complementary techniques have allowed an easy identification of the main anionic species found in the glasses: metaphosphate, $(PO_3)^-$, pyrophosphate, $(P_2O_7)^{4-}$, and orthophosphate groups $(PO_4)^{3-}$ and how they are affected by the different modifier cations nearby.

Vitreous P_2O_5 is formed by Q^3 groups where the P=O bond, establishing a weaker network, is highly hydrophilic, being the reason for the high retention of water in the form of P-OH bonds in phosphorus pentoxide as well as for ultraphosphate glasses.

The introduction of modifier oxides breaks up the P-O-P bonds and forms P-NBO bonds with terminal oxygens linked to modifier cations. Once the metaphosphate composition is attained only chains or rings of Q^2-type groups remain. With further additions of a modifier, the Q^2 convert to Q^1 and depolymerize the structure until orthophosphate (PO_4^{3-}) species.

In a more general perspective, Brow conducted a comprehensive review of the structure of phosphate glasses by exploring all the important factors [8].

Phosphates have also been studied in the form of glass-ceramics trying to reproduce the composition of crystalline compounds [9-13]. An example, based on lithium titanium

phosphates with the NASICON (sodium superionic conductor) type structure, is given in ref. [14]. Glasses, within the Li_2O-Al_2O_3-MO_2-P_2O_5 composition diagram where M can be Ge or Ti, were prepared through a melt-quenching method at temperatures from 1400 to 1500ºC and then heat treated in order to develop the LATP crystalline phases and they all belong to the orthophosphate composition. Normally, they should give rise to fully crystallized materials, but the melts have a very high tendency for spontaneous crystallization given the very low amount of P_2O_5 in their chemical formulation. As a consequence, they result in inhomogeneous glass/glass-ceramics. Nevertheless, these materials reach room temperature conductivities of about 10^{-4} $S.cm^{-1}$, which allow them to be used as solid-state electrolytes in their bulk form. These LATP glass-ceramics have been tested into lithium-air secondary batteries as a protecting layer of the lithium metallic electrode [15]. Another example was achieved by Abe and co-workers [16] who prepared porous glass-ceramic in the CaO-P_2O_5-TiO_2-Na_2O system. They used a method analogous to the production of porous glass by acid leaching a phase separated glass-ceramic. Heat treatment of a specific glass composition yielded to crystallization of $CaTi_4(PO_4)_6$ and $\beta Ca_3(PO_4)_2$. The latter phase was leached with acid giving a porous skeleton of the other phase with have an excellent chemical durability.

In order to develop glass-ceramics that have desirable properties, it is of importance to control the crystallization process so that an even distribution of crystals can be formed. This is done by controlling the nucleation and crystal growth rate which are both function of temperature.

The aim of the crystallization process is so that the glass-ceramics has better properties than the parent glass. However, the impact of the thermal history and partial to full crystallization on the glass reactivity is of great interest. It has been demonstrated [17] that a change in overall thermal history does not impact the in vitro reactivity as long as no clear crystallization occurs. If crystals are present at the particle surfaces, the precipitation or adhesion of a CaP reactive layer is inhibited just as the bioactivity.

Nevertheless, crystallization is known to affect material's stiffness and generally enhances mechanical characteristics. Also, the knowledge of the crystallization mechanism and of the kinetics are critical in determining those glass compositions that can be converted into practical fine grained glass ceramics. In the same way, the nucleation rate and its temperature dependence in glass forming melts are not only of great scientific importance to understand glass formation, but are also of practical interest for this purpose.

However, investigations in this area concern essentially silicate or aluminosilicate glass compositions in contrast to the few studies dealing with phosphate glasses.

Consequently, in this study, we carried out investigations about the congruent crystallization of several glass phosphate compositions characterized by different values of the O/P ratio. For a metaphosphate composition (O/P = 3), we focused on $LiPO_3$ which is less sensitive to moisture than the sodium metaphosphate, thus water or hydroxyl groups do not affect the crystallization phenomenon at the experimental time scale. $Sn_2P_2O_7$ was chosen as the pyrophosphate composition (O/P=3.5) and $LiGe_2(PO_4)_3$ as the orthophosphate composition (O/P=4). All these glasses are easily vitrified by the melting and quenching method.

The objective was threefold: (i) to get information on the dominant crystallization mechanism (i.e. surface or volume) by using the analytical method developed by Ray et al. [18], (ii) to determine the kinetic parameters of the overall crystallization phenomenon (the activation energy for crystallization and the Avrami exponent) from non-isothermal experiments according to the Ozawa's method [19], (iii) to test how well the adiabatic theory developed by Meyer [20] can predict the temperature of the maximum nucleation rate.

2. Analytical

It has been previously shown that differential thermal analysis (DTA) could be used to determine the dominant crystallization mechanism in glass [5]. In this DTA method, δT_p (the maximum height of the DTA peak at T_p) which is expected to be proportional to the total number of nuclei, is plotted as a function of the glass particle size, with both the amount of sample and the heating rate remaining constant. For a fixed amount of sample, the ratio of

the volume to the total effective surface area of all glass particles increases with increasing the particles size. For internal (or surface) dominant crystallization, δT_p should increases (or decreases) with increasing the particles size.

Likewise, DTA can be considered as a rapid and convenient means of determining nucleation–rate type curves, especially the temperature and time dependence [21]. Hence, for a given particle size, T_n^{max}, the temperature where the nucleation rate is maximum is determined from the plot of the crystallization peak height δT_p as a function of the nucleation temperature T_n , the nucleation time t_n, the weight sample and the heating rate β being constant for each DTA scan. In addition, the changes in δT_p at T_n^{max} with nucleation time are expected to indicate when the glass is saturated with nuclei.

Isothermal devitrification is well described by the Avrami's law:

$$x = 1 - exp[-kt^n] \quad (1)$$

where x is the volume fraction crystallized after time t at a fixed temperature T, n is the Avrami exponent and k is defined as the apparent reaction rate, which is usually assigned an Arrhenian temperature dependence:

$$k = k_0 \exp\left[-\frac{E_a}{RT}\right] \quad (2)$$

where E_a is the activation energy describing the overall crystallization process.

After rearrangement of eq.(1), one obtains:

$$Ln[-Ln(1-x)] = Ln(k) + n.Ln(t) \quad (3)$$

The corresponding plot is a straight line, the slope gives directly the value of n and the intercept yields to the value of the reaction rate k. After several isothermal experiments conducted at different temperatures, the plot of $ln(k)$ as a function of $1/T$ gives the value of the activation energy.

It should be noted that eq.(1) strictly applies to isothermal studies. However, it is commonly used to describe non-isothermal crystallization for which experimental studies are easier to conduct. Several different treatments have been summarized by Yinnon and Uhlmann [19]. All these methods are based on eq.(1) and eq.(2) and assume a constant heating rate β in all

DTA or DSC experiments. On this basis, plotting $Ln[-Ln(1-x)]$ versus $Ln(\beta)$ at a fixed temperature, yields to the value of *n*, the relation being written as:

$$\frac{d[Ln[-Ln(1-x)]]}{d[Ln(\beta)]} = -n \quad (4)$$

For the determination of the apparent activation energy for crystallization E_a, we used the he the Ozawa method [43] by the following equation:

$$\frac{d[Ln(\beta)]}{d[1/T_p]} = -\frac{E_a}{R} \quad (5)$$

where T_p is the crystallization peak temperature at the heating rate β.

The classical nucleation theory is based essentially on three hypotheses: (i) nucleation is an isothermal phenomenon; (ii) nucleation appears as a result of heterofluctuations; (iii) the interfacial tension does not depend on the radius of the nucleus. The first two hypotheses are related and have to be accepted together or not. The idea is that nucleation is a nonspontaneous phenomenon, resulting from an equilibrium distribution of heterofluctuations. However, if it is reasonable to admit that nucleation is an isothermal phenomenon, the existence of such heterophase fluctuations never has been proven experimentally. Consequently, the question arises whether nucleation could not be a spontaneous adiabatic phenomenon. This theory, developed by Meyer [20] stipulates the following assumptions:

(i) $C_p = \frac{(C_p^l + C_p^s)}{2}$ is a constant, where (C_p^l) and (C_p^s) are the molar specific heats of the liquid and solid phases at the melting point, respectively

(ii) the solid/liquid interfacial tension is size dependent and is given by Tolman's equation [23]

$$\frac{\sigma}{\sigma_\infty} = (1 + 2\,\delta/r)^{-1} \quad (6)$$

where δ is roughly equal to half of the intermolecular distance and *r* is the radius of the nucleus

(iii) the melting enthalpy is size dependent

(iv) the number of molecules of the adiabatic nucleus is that of a Wigner-Seitz primitive cell (N_w)

(v) statistical temperature fluctuations are considered instead of isothermal heterophase fluctuations.

Considering $x = \frac{\Delta_m S}{C_p}$ where $\Delta_m S$ and C_p are the melting entropy and the heat capacity per mole, this theory, fully discussed by Meyer [20], gives a maximum supercooling temperature for liquids (T_{Nw}) which are supercooled in relation to solid phases having a Wigner-Seitz number N_w :

$$\frac{T_{Nw}}{T_m} = x\left[1 - \left(\frac{R}{C_p Q N_w}\right)^{0.5}\right]^{-1}\left(1 + \frac{2\delta}{r}\right)^{-1}[e^x - 1]^{-1} \qquad (7)$$

Where C_p is the specific heat of the supercooled liquid and Q is the number of atoms per molecule of the solid phase and k is the Boltzmann's constant. N_w is the number needed to define the Wigner-Seitz primitive cell which is 13 for a *fcc* or *hcp* structure and 15 for a *bcc* structure. A mean value of about 14 was chosen in the case of the glass nucleation.

Nevertheless, the specific heats of supercooled liquids are not expected to vary so much in the temperature range from $0.5T_m$ to T_m and eq. (7) is not very sensitive to variations of C_p, hence the value at melting temperature can be used as well.

The Tolman's parameter (2δ) being about the intermolecular distance, such a Wigner-Seitz primitive cell, which determines the group of molecules (approximately spherical), is considered to have a radius of 3δ. Using these approximations, one finally obtains:

$$\frac{T_{14}}{T_m} = \frac{3}{5}x\left[1 - 1\left(\frac{R}{14Q}\right)^{0.5} {C_p}^{-0.5}\right]^{-1}[e^x - 1]^{-1} \qquad (8)$$

Moreover, C_p does not vary a lot from element to element and can be substituted by 3R according to the Dulong-Petit rule. This leads to the following equation:

$$\frac{T_{14}}{T_m} = x[1.67 - 0.26\, Q^{-0.5}]^{-1}[e^x - 1]^{-1} \qquad (9)$$

Theoretically, the value of this ratio is in the range given by eq. (10). As an evidence, an infinite value for Q gives the lower limit while the upper limit corresponds to $Q = 1$.

$$x[1.67]^{-1}[e^{x}-1]^{-1} < \frac{T_{14}}{T_m} < x[1.41]^{-1}[e^{x}-1]^{-1} \qquad (10)$$

This simple adiabatic nucleation model, based on an extended enthalpy-entropy diagram, predicts a definite stability limit for the liquid-solid phase transition and is in good agreement with the experimental supercooling temperatures of low viscosity liquids such as in the case of liquid gallium.

Zanotto generalized this theory to the case of multi-component glasses [22]. However, he didn't use the Dulong-Petit rule because of the number of different atoms characterizing such glass compositions. Consequently, eq. (8) becomes:

$$\frac{T_{14}}{T_m} = x\left[1.67 - 1.28Q^{-0.5}{C_p}^{-0.5}\right]^{-1}[e^{x}-1]^{-1} \qquad (11)$$

The nucleation probability is relatively high at T_{14} and has a strong increasing tendency as the temperatures decreases. Assuming that the maximum supercooling temperature is close to the temperature of maximum nucleation rate, one can estimate T_{max} by means of T_{14}. The calculation of T_{14} is easy when compared to that of T_{max} by means of the classical nucleation theory.

In the following sections, the maximum supercooling temperature (T_{14}) will be considered as T_{max} the temperature for which the nucleation rate is at maximum, the calculation being made by using eq. (9). However, it remains a question about the value of *Q*. Considering the case of polymers, Meyer [20] assumes, as an evidence, that *Q* does not correspond to the total number of atoms of the macromolecule, but to the number of atoms of the monomer as indicated by the chemical formula. Undeniably, the case of a multi-components glass differs from that of a polymer, consequently for the *Q* values, we will take into consideration the number of molecules per unit cell of the crystalline phase.

3. Experimental

Glass synthesis

Concerning the metaphosphate and the pyrophosphates glasses, a two-step process has been preferred. Commercial reagents of ammonium phosphate ($NH_4H_2PO_4$), lithium carbonate (Li_2CO_3) or tin oxide (SnO) were mixed in appropriate proportions and heated, step by step, up to 500°C inside an open furnace to remove water, ammonia and carbon dioxide when carbonate is used. This temperature was maintained during 10h and then, the sample was cooled down to room temperature into the furnace, giving a crystalline powder.

Glass compositions of about 30g were prepared by the conventional melting and quenching method. The crystalline powder was heated within a silica crucible during 10 min. by means of a microwave heating device with a nominal power of 750 W. The temperature of the melt was monitored using an optical pyrometer. Then the melt was poured on a stainless steel mold, annealed close to T_g, and slowly cooling down to room temperature. All the glasses were stored in a desiccator and prior to their physical characterization, the chemical composition was checked by means of Energy Dispersive Spectroscopy (EDS analysis) to ensure that no trace of silica was found in the samples.

In the specific case of the orthophosphate glass composition and due to the higher temperature required for the melting, a one-step process was preferred. Ammonium phosphate ($NH_4H_2PO_4$), lithium carbonate (Li_2CO_3) and germanium oxide (GeO_2) were heated in a platinum crucible, up to 1300°C inside a muffle furnace. To avoid the phosphorus release at this temperature, the melting time was of about 30 min and then, the rest of the procedure was strictly identical to that described for the other glass compositions.

Thermal analysis

All the glass samples used in this study were coming from a single piece of glass. DSC scans (NETZSCH STA 449 F3) were conducted on specimens contained in a Pt pan. A Pt pan with sapphire was used as a standard. Temperature calibration was carried out over a large range employing high purity materials approved by the Committee on Standardization of the International Confederation for Thermal Analysis (ICTA) [21]. The overall accuracy of this measurement is expected to be within ± 2°C.

To determine the dominant crystallization mechanism in glass, the bulk glasses were ground and sieved to 7 different particle size ranges, < 20, 20–38, 38–63, 63–100, 100–200, 200–315, 315–500 µm. These different ranges are designated by the approximate average size in each range (excepted for the first one): 10, 29, 50.5, 81.5, 150, 257.5 and 407.5 µm. Consequently, samples of different particle sizes, with a constant weight (30 ± 0.1 mg) were heated at 15°C.min^{-1} from room temperature until crystallization was complete. This should avoid the possible overlapping of the nucleation and growth phenomena. The estimated experimental error in the measurement of δT_p does not exceed ± 3%.

Although a reasonably long nucleation time (t_n) is recommended for accurate DSC experiments, the primary purpose is to develop some nuclei, that produce a measurable crystallization peak in order to determine the T_n^{max}. Hence, the most important experimental parameters are to use the same nucleation time (1h in this case) and a reasonably high heating rate (15°C.min^{-1}) to ensure that no new nuclei will be formed during this non-isothermal treatment.

In addition, all the kinetic parameters of the non-isothermal devitrification were determined from DSC experiments conducted at heating rates in the range 5-20°C/min. The crystallized volume fraction, at a given temperature, was determined from the relative area of the crystallization peak.

From an experimental point of view, the adiabatic theory requires to determine the melting temperature and the corresponding enthalpy in addition to the heat capacity temperature dependence. For this purpose, DSC scans were conducted according to the DIN 51007 method available with the NETZSCH Proteus 6.1.0 thermal analysis software. This method is similar to the ASTM E 1269 and ISO 11357-4 and requires the same temperature program with isothermal segments before and after the dynamic segment performed at 20°C.min^{-1}. Nevertheless, DIN 51007 requires additionally the interpolated baseline of the measured DSC signal between the two isothermal segments. The better the reproducibility of the baselines, the better this interpolation is constant at zero. Pt crucibles with lids and sapphire as the standard were used for analysis of all bulk samples with a weight equivalent to that of

sapphire (30 ± 0.3 mg). Prior to these thermal analysis, a sensitivity curve was determined from a calibration measurement over the whole temperature range of the instrument.

Phase identification

To identify the phases after devitrification of the synthesized glasses, vitreous samples were heated up to the maximum of the crystallization temperature at a heating rate of 10°C·min^{-1} and then slowly cooled down to room temperature by turning off the furnace. After grinding and sieving, the treated samples with a particle size from 100 to 200 µm, were mounted in a rotating holder with a 27-mm-diameter ring. XRD experiments were performed on the Panalytical X'Pert Pro diffractometer with a Cu Kα anode tube operating at 40 kV/40 mA; the detector used was the X'Celerator, using real-time multiple strip (RTMS) position-sensitive detection technology, which enables faster data collection than a conventional point detector. The scans were performed from 5° to 120° (2θ) with a step size of 0.026° (2θ) and counting times of 40 s per step to ensure satisfactory counting statistics.

Physical characteristics

Helium pycnometry was used to determine the specific weight of the glass samples and of their corresponding crystalline structure. The density precision is of ± 0.02 g.cm^{-3}. From the density difference, one can calculate a value for the density misfit parameter, Δ_d, given by the following equation:

$$\Delta_d = \frac{(d_c - d_g)}{d_g} \text{ in } \% \qquad (10)$$

where d_c and d_g are the crystal and the glass densities, respectively. This parameter determines the magnitude of the elastic stresses in the crystallization process [24].

The coefficient of thermal expansion (CTE) was measured using a TMA analyzer (TA Instrument 2940) with a preload force of 0.1 N and a heating rate of 5°C.min^{-1} (precision: ± 2.10^{-7} K^{-1}).

4. Results

4.1 Glass synthesis

Glass synthesis of the metaphosphate and of the pyrophosphate have been performed using a domestic microwave oven. As illustrated by Fig.1, the maximum temperatures, which are close to 700°C and 900°C for $LiPO_3$ and $Sn_2P_2O_7$ respectively, are reached very quickly (less than 100s) and the synthesis can be considered as stable within 5 minutes.

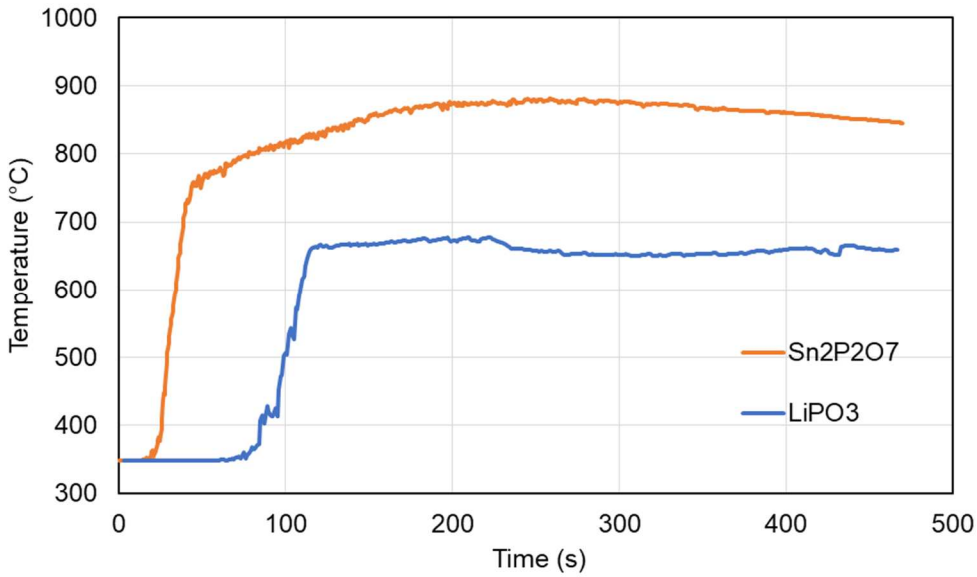

Figure 1 : Temperature profile for glass synthesis under microwave irradiation

As mentioned in the above section, the orthophosphate glass was prepared using a conventional heating device, due to the higher temperature required for melting the batch. Fig.2 shows the very strong tendency to devitrification of this composition as illustrated by the temperature to time dependence. The glass crystallization occurs just after the glass transition and this sharp exothermic event is responsible of a quick increase of temperature of about 15°C detected by the sensor and shown in the inlet. An instant heating rate of more than 200°C.min^{-1} is also measured. Such an intense devitrification phenomenon imposes a fast quenching rate to produce a bulk glass of about 30g.

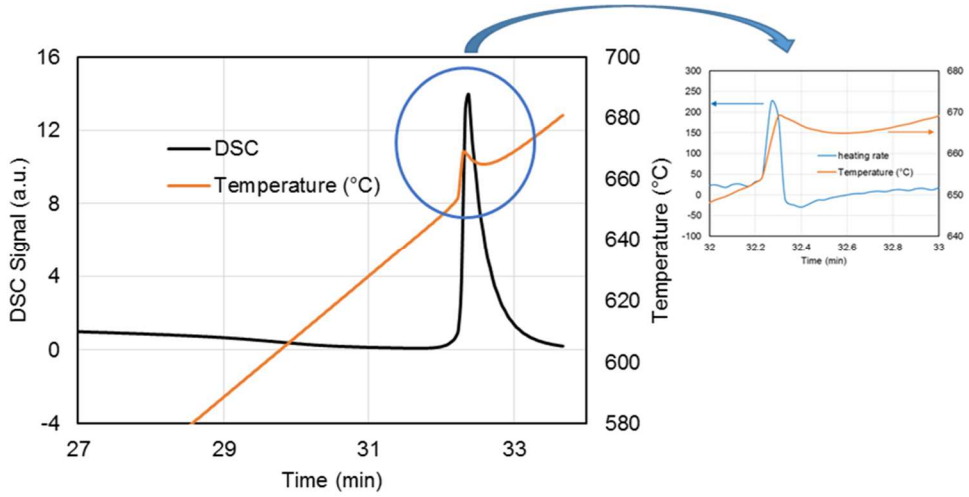

Figure 2: DSC trace at 20°C.min^{-1} and temperature to time dependence for the $LiGe_2(PO_4)_3$ glass (exo up) – Inlet depicts the instantaneous heating rate and the temperature of the sample.

4.2 Glass characterization

Table I summarizes several physical characteristics of bulk glass samples, except the density of the crystals which has been measured on powder samples. The characteristic temperatures have been determined at a heating rate of about 20°C.min^{-1}. As expected, the characteristics temperatures of the pyrophosphate glass are remarkably low while those of the orthophosphate are similar to those of silicate glasses. The density of the glasses varies from 2.35 to 3.74 clearly depending on the atomic weight of the heaviest element of the glass composition (Sn>Ge>Li). The coefficient of thermal expansion of the orthophosphate is low compared to the other values or what is generally expected for phosphate glasses. It should be noticed that these values are mean values and have been determined from room temperature to T_g. The density misfit parameter varies from 4 for the metaphosphate to a values 2.5 times higher for the orthophosphate.

Table I : Physical characteristics of the glasses

	T_g (°C)	T_p (°C)	T_m (°C)	T_g/T_m calc. in K	d_c g.cm^{-3}	d_g g.cm^{-3}	$\alpha.10^{-6}$ K^{-1}	Δ_d %
$LiPO_3$	313	440	653	0.633	2.45	2.35	18.2	4
$Sn_2P_2O_7$	274	380	619	0.613	4.04	3.74	14	8
$LiGe_2(PO_4)_3$	576	670	1230	0.565	3.53	3.20	7	10

4.3 Phase identification

Figure 3 displays the X-rays diffraction patterns obtained for the crystallized samples. Phase identification was not ambiguous for the metaphosphate and the orthophosphate compositions. It matches well to the $LiPO_3$ monoclinic phase (ICDD PDF 2 n° 70-0274) and to the $LiGe_2(PO_4)_3$ rhombohedral phase (ICDD PDF 2 n° 80-1922) respectively. In the case of the pyrophosphate composition, the interrogation of the database was not successful due to the absence of relevant crystallographic data concerning $Sn_2P_2O_7$. However, the diffraction pattern matches well with the $\beta Sn_2P_2O_7$ phase, with a triclinic symmetry, described in [25].

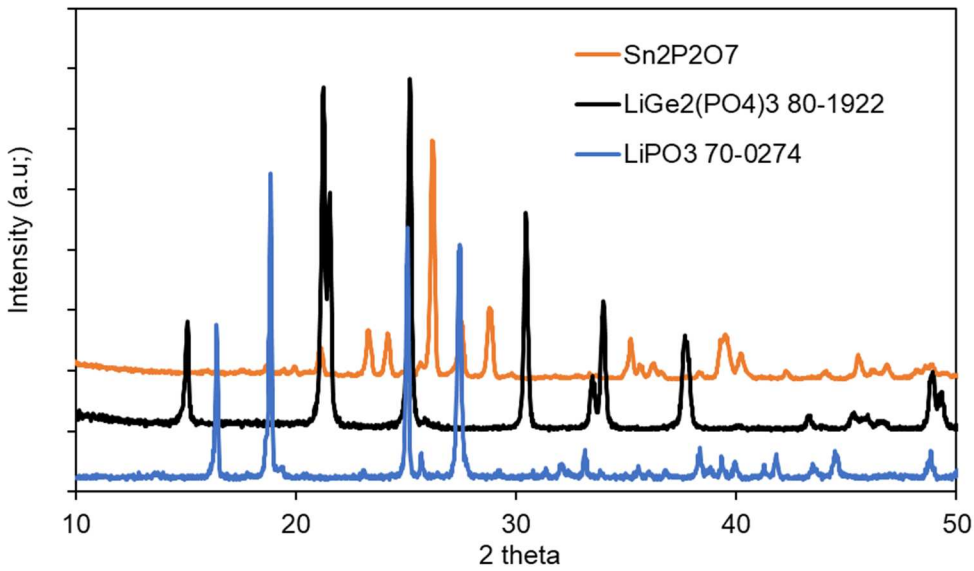

Figure 3: X-ray diffraction patterns of the crystallized samples – ICDD PDF 2 references are given when available

4.4 Nucleation analysis

The effect of particle size on the intensity of the DTA crystallization peak is shown in Fig. 4. For the $LiPO_3$ glass, the DTA peak height is clearly decreasing with the particle size of the sample suggesting a surface dominant nucleation. Such a behavior cannot be put in light in the case of the other glasses which do not present such a dependence.

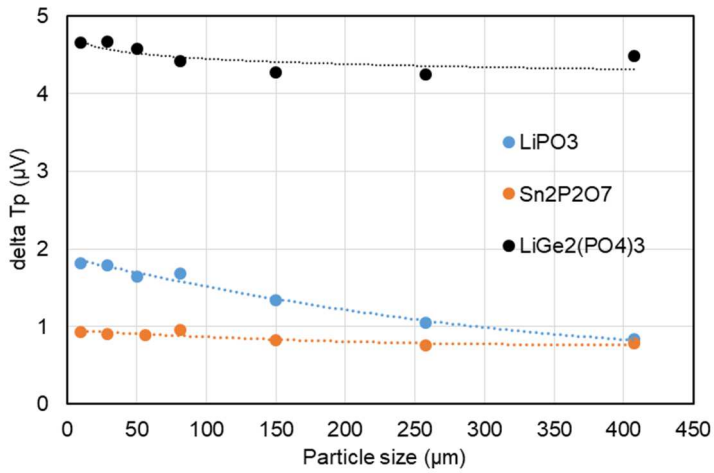

Figure 4 : DTA peak height as a function of the particle size of the sample

As a result, nucleation occurs simultaneously at the surface and in the volume of the samples.

The dependence of the nucleation in terms of temperature is shown in Fig. 5. Samples have been nucleated at various temperatures, the nucleation time (1h), the weight (30mg), the heating rate (15°C.min^{-1}) and the particle size range (315-500µm) of the samples being constants. The choice of the large particle size was made in order to model the crystallization of a bulk sample (i.e. to have an infinite size sample).

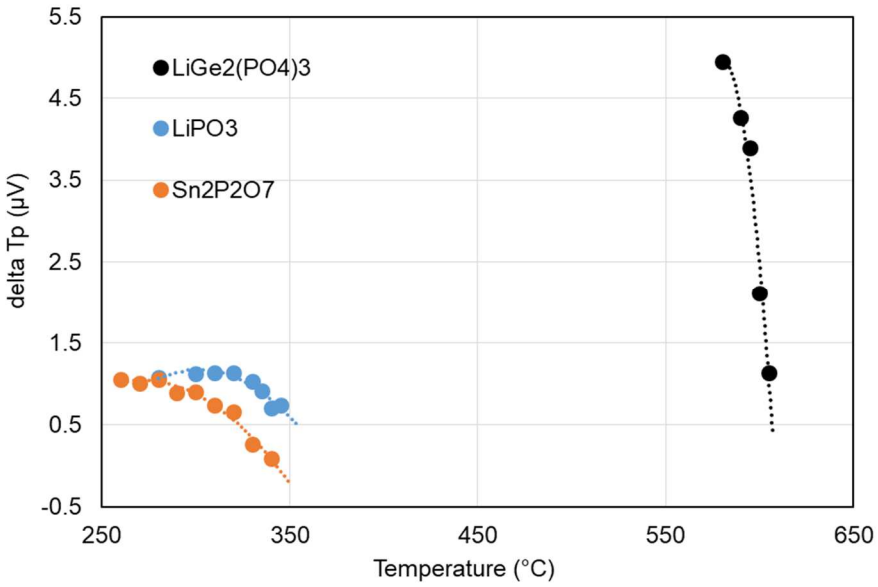

Figure 5: DTA peak height as a function of the nucleation temperature for a nucleation time of 60 minutes

δT_p, which represents the total number of nuclei, is constant for nucleation heat treatment conducted at temperatures below T_g and then drastically decreases above T_g, indicating the absence of an optimal nucleation temperature.

These assumptions are corroborated by the following SEM pictures, depicting the crystallization behavior of bulk samples after nucleation heat treatments. Fig. 6a illustrates, in the case of the $LiPO_3$ glass, the crystallization occurring from the surface of the bulk and extending towards the core of the sample.

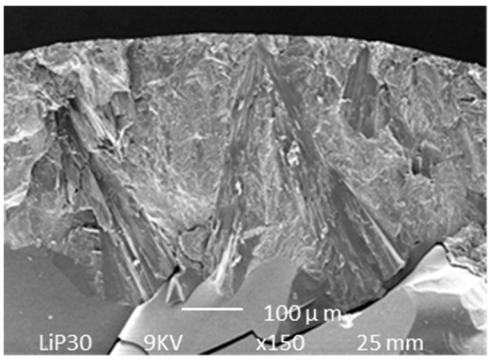

Figure 6a: SEM picture of $LiPO_3$ crystallized glass (T_n = 400°C – t_n = 30 min – X150)

The case of the pyrophosphate and of the orthophosphate are at the opposite. Figs. 6b and 6c clearly show that crystallization occurs throughout the sample and not only at the surface, even though the nucleating time is shorter than in the case of the metaphosphate (10 min vs 30 min).

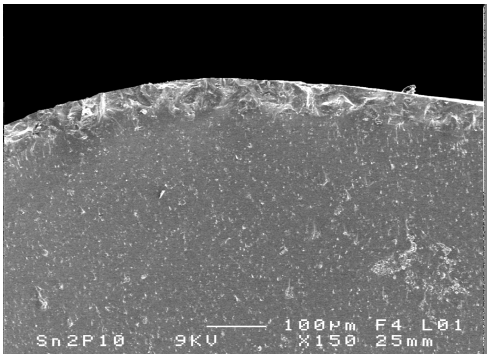

Figure 6b: SEM picture of the $Sn_2P_2O_7$ crystallized glass (T_n = 360°C – t_n = 10 min – X150)

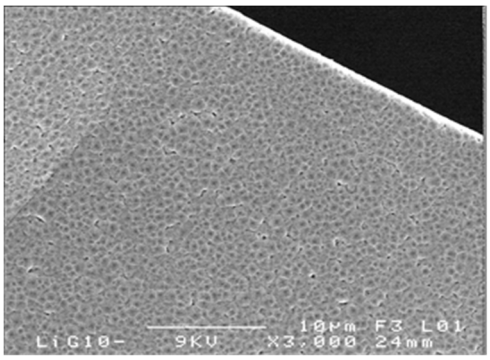

Figure 6c : SEM picture of the $LiGe_2(PO_4)_3$ crystallized glass (T_n = 620°C – t_n = 10 min – X3000)

Thus, for the following experiments, no specific nucleation heat treatments were performed to determine the kinetics of the overall crystallization phenomenon.

4.5 Non-isothermal crystallization

Non-isothermal studies were conducted from DSC experiments according to the analytical methods described in section 2.

The Avrami exponent was determined, by plotting eq. (4) at various temperatures depending on the glass compositions. In the present work, only values corresponding to a limited

crystallized volume fraction were employed, i.e. less than 0.5. This helps to minimize the influence of complicating factors which occur during the later stages of crystallization, particularly the restriction of crystal growth by the finite size of the glass particles. As expected, the different plots give straight lines and the slopes yield to values of the Avrami exponent which are summarized in Table II with the corresponding correlation coefficients. It results that the exponent value is of about 2 for the metaphosphate and increases slightly (2.4) for the pyrophosphate and stronger for the orthophosphate (4.1). Concerning the activation energy of the overall crystallization, the different plots from the Ozawa's relation (see eq. 5) yield to straight lines. From the slopes, one obtains the values of E_a which are given in Table II with the corresponding deviation. These values increase from 127 kJ.mole^{-1} for the metaphosphate to 140 kJ.mole^{-1} for the pyrophosphate and 358 kJ.mole^{-1} for the orthophosphate.

Table II : Avrami exponent and activation energy values from non-isothermal Ozawa's equation

	T (°C)	425	430	435	440	<*n*>	E_a(kJ.mol^{-1})
$LiPO_3$	*n*	2.23	2.19	2.18	2.10	2.18 (0.06)	127 (5)
	R^2	0.994	0.982	0.994	0.990		
$Sn_2P_2O_7$	T (°C)	360	365	370	375		
	n	2.39	2.44	2.41	2.32	2.39 (0.05)	140 (5)
	R^2	0.998	0.998	0.996	0.994		
$LiGe_2(PO_4)_3$	T (°C)	665	670	675	680		
	n	5.40	4.67	4.05	3.61	4.1	358

	R^2	0.994	0.991	0.929	0.920	(0.7)	(5)

4.6 Adiabatic nucleation analysis

As mentioned above, the determination of the heat capacity temperature dependence with the best precision is of primary importance. This can be achieved by strictly respecting the protocol described in the experimental section. Fig. 7 illustrates a typical C_p versus temperature curve obtained in the case of the pyrophosphate glass, the others compositions present similar type curves. As expected, the specific heat capacity increases gradually from room temperature to T_g. On passing through the glass transition to the supercooled liquid state, the heat capacity increases by a factor of about 1.4 which is in the range usually admitted (i.e. from 1.2 to 1.8) [26]. This behavior reflects the increase in configurational entropy, which becomes possible in the supercooled liquid state [27]. After melting, the C_p values for the liquid state can be considered as temperature independent in the short temperature range explored. The melting temperature and the corresponding enthalpy are easily determined from the C_p curve. In addition, one can see on Fig. 7 that the values of the crystallization enthalpy and of the melting enthalpy are quite the same.

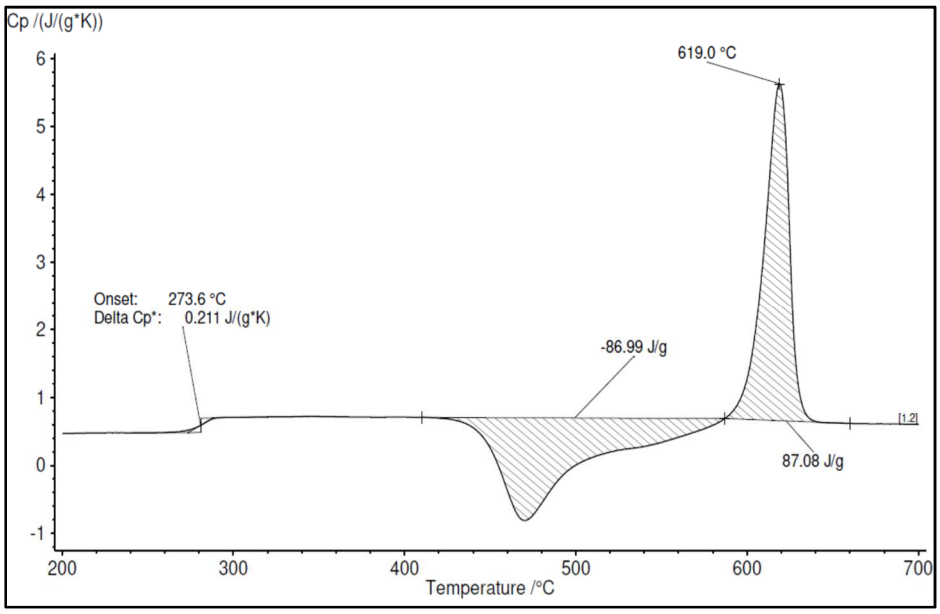

Figure 7: Heat capacity temperature dependence for the $Sn_2P_2O_7$ glass composition

Eq. (10) gives the limits of the reduced temperature of maximum nucleation as a function of the dimensionless parameter ($\Delta_m S/C_p$). As a result, the (T_{max}/T_m) values calculated from eq. (9) should lie in this range. This is illustrated by Fig. 8 which clearly shows that this relative temperature, decreases for glasses which combine both high values of melting entropy and low values of heat capacity. In addition, the calculated values of this reduced temperature for several glass compositions are also depicted in order to cover, as far as possible, the widest range of *x* values. According to data issued from literature [22, 28], some of them are known to present an internal nucleation, i.e. Na_2SiO_3, $BaSi_2O_5$ and $Li_2Si_2O_5$. Regarding to our observations, $LiGe_2(PO_4)_3$ and $Sn_2P_2O_7$ belongs to this category. The others present only surface nucleation, i.e. $CaAl_2Si_2O_8$, SiO_2, B_2O_3 and $LiPO_3$ which belongs to this group. The data relative to the crystalline counterpart which are used for the calculation of the *Q* parameter are given in Table III.

Table III: Crystallographic data from ICDD PDF 2 Database except for $Sn_2P_2O_7$ [25]

(Calculated densities – Molecular weight – Cell volume – Number of molecules in the unit cell)

	Na_2SiO_3	$LiPO_3$	$Li_2Si_2O_5$	SiO_2	$CaAl_2Si_2O_8$	B_2O_3	$BaSi_2O_5$	$LiGe_2(PO_4)_3$	$Sn_2P_2O_7$
d ($g.cm^{-3}$)	2.624	2.46	2.456	2.331	2.736	2.558	3.768	3.587	4.088
M (g/mole)	122.06	85.91	150.05	60.08	278.21	69.62	273.5	437.04	411.36
V ($Å^3$)	154.3	1159.9	405.8	171.2	675.5	135.5	481.7	1213.9	668.2
Z	2	20	4	4	4	3	4	6	4

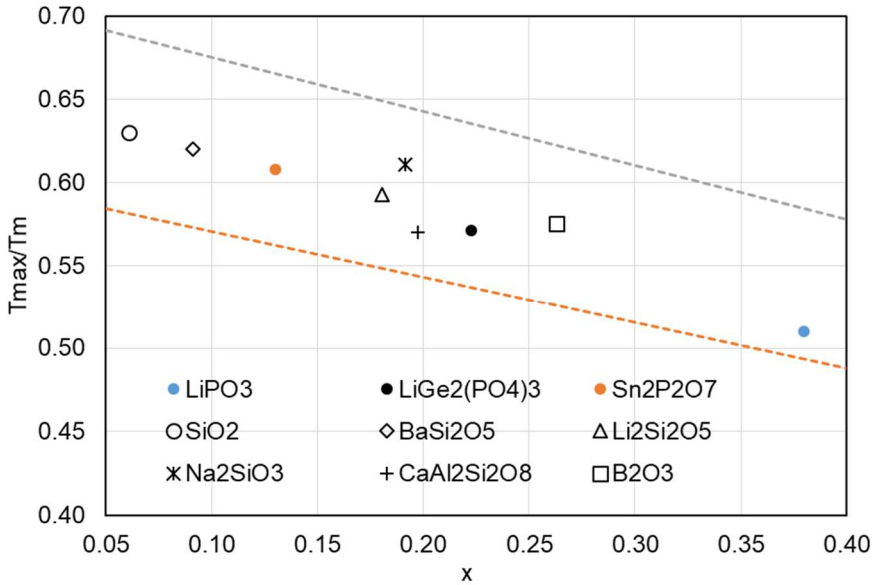

Figure 8: Reduced temperature of maximum nucleation as a function of the dimensionless parameter ($x = \frac{\Delta_m S}{C_p}$)

The values of T_{max}/T_m, calculated by adiabatic theory, are plotted as a function of the reduced glass transition temperature and depicted in fig. 9. This figure also shows the line for $T_{max} = T_g$ and can be divided in two areas, the points located at the left side of the line are representative of glasses for which $T_{max} > T_g$ and correspond to glasses which are experimentally known to crystallize internally, whereas those at the right side represent glasses, for which $T_{max} < T_g$, crystallize only from the surface.

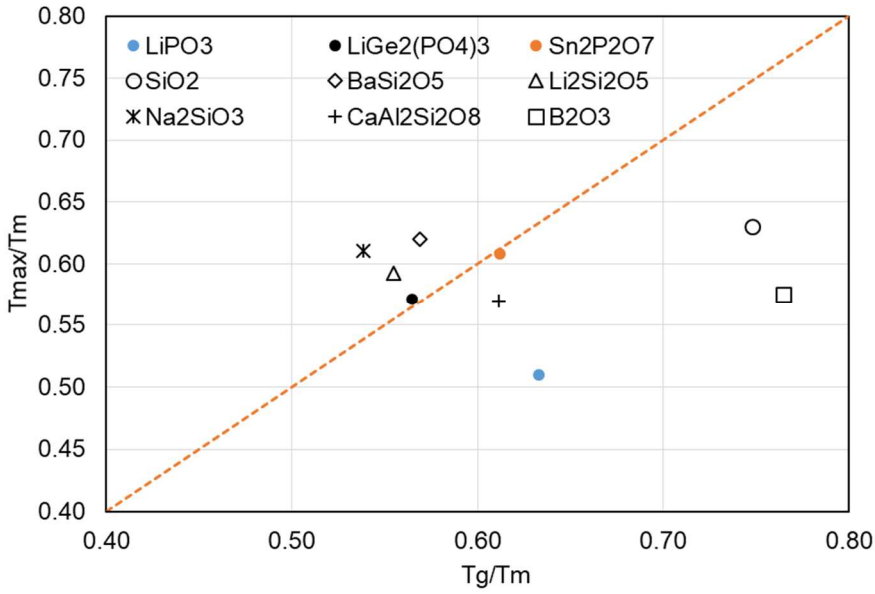

Figure 9: Reduced temperature of maximum nucleation, according adiabatic theory, versus the reduced glass transition temperature

As expected, the metaphosphate is clearly belonging to the right domain and crystallizes only from surface, whereas the orthophosphate belongs to the left domain and crystallizes internally. The case of the pyrophosphate is more ambiguous and suggests that crystallization occurs both from surface and volume as observed experimentally.

5. Discussion

Nucleation analysis

The effect of particle size of the glass sample on the height of the crystallization peak is clearly illustrated by Fig. 4. A strong dependence with the mean diameter of the particles, as observed for $LiPO_3$, suggests a surface dominant nucleation. Such a dependence is not noticed for the other glass compositions. Paying attention to a maximum relative deviation of about 3% in the experimental data, one can assume that the DTA peak heights are constant, with mean values of about 0.86 µV and 4.58 µV for $Sn_2P_2O_7$ and $LiGe_2(PO_4)_3$, respectively.

According to [18], the use of large glass samples makes it possible to neglect surface crystallization for analyses of overall crystallization kinetics. In addition, it was also shown that internal crystallization in lithium disilicate glass dominates over surface crystallization when the glass particle size exceeds 300 nm. Consequently, the temperature dependence of the nucleation rate was determined from the DSC peak height and shown in Fig. 5. The absence of an optimal temperature seems to indicate that internal nucleation was not effective, even after a heat treatment of about 1h at various temperatures. Indeed, if a glass does not undergo internal nucleation or if this phenomenon is very weak, surface crystallization dominates whatever the particle size. According to [29], this characteristic size is a relative quantity that depends on the magnitude of the internal nucleation rate and of the time and temperature dependence. Furthermore, it has been stated [30] that the peak height method is only valid under certain conditions and among these, the possible overlap between the nucleation and growth phenomena can impede an accurate qualitative analysis of nucleation kinetics. Nevertheless, SEM pictures, given in Fig. 6, illustrate the difference in crystallization behavior between the studied compositions. Evidence of an internal nucleation was pointed out in the case of $Sn_2P_2O_7$ and of $LiGe_2(PO_4)_3$.

Non-isothermal crystallization

As mentioned in the experimental section, the kinetic parameters of the non-isothermal crystallization were determined from glass powders with a particle size range between 315 and 500µm. This should allow to consider the glass particle size as infinite regarding to the crystal growth. The Avrami exponent, which describes the overall crystallization phenomenon, is slightly above 2 for the metaphosphate. Knowing that nucleation occurs heterogeneously and instantaneously at the surface of the glass, crystallization should be 2D and crystal growth should be limited by the development of the glass to crystal interface yielding to an Avrami exponent between 2 and 3. This is corroborated by information from SEM picture (Fig.6a). Considering the pyrophosphate glass, a similar value of the Avrami exponent should yield to the same conclusion. However, the situation is a little bit different as

illustrated by Fig. 6b. If crystallization occurs first from the glass surface, giving sense to heterogeneous nucleation. There is also an indication for homogeneous nucleation, despite a shorter nucleation time, yielding to a 3D growth from a constant number of nuclei and to an increase of the Avrami exponent. Generally speaking, the observation of homogeneous nucleation is a matter of having nucleation time lags short enough when compared to the laboratory time scale.

As mentioned in the introduction section, there have been relatively few studies of glass ceramics formation in phosphate systems and it has been settled that volume nucleation was difficult to promote [31]. Nevertheless, it has been shown that addition of B_2O_3, contrary to Al_2O_3, can promote volume nucleation in calcium phosphate glasses in the series (100-*x*)CaO-P_2O_5-*x*B_2O_3, nevertheless this only occurs for *x* in the range from 15-25 mol.%. Outside this range, only surface crystallization occurs. The orthophosphate glass composition doesn't show the same behavior. The values of the Avrami exponent clearly indicate that crystallization is 3D and this is corroborated by the SEM picture given in Fig. 6c. Moreover, these values are greater than 3 and suggest that crystal nucleation and growth curves overlap extensively.

This was previously observed in [32] and a value of about 3.8 was given for the same glass composition. However, the Avrami exponent was determined using the Augis-Bennett equation [19].

$$n = 2.5\frac{RT_p^2}{(\Delta T)E_a} \quad (12)$$

where T_p is the temperature of the crystallization peak, ΔT is the width at mid-height of the exothermic peak in the DSC curve and E_a is the crystallization activation energy which was previously calculated from the Kissinger equation, β being the heating rate :

$$\frac{d[ln(\beta/T_p^2)]}{d[1/T_p]} = -\frac{E_a}{R} \quad (13)$$

The fact that the *n* values (determined from eq. 4) are different from 1 indicates that surface crystallization is not the dominant mechanism. As a consequence, the activation energy for crystallization should not be calculated from the Kissinger equation which was derived for unidimensional growth.

Considering the activation energy for crystallization, the Ozawa method uses the shift of the crystallization peak temperature to a higher value with an increase in the heating rate. Such a shift implies the presence of a high concentration of nuclei at low heating rates because of the longer time for nucleation. Consequently, crystallization occurs in a shorter period of time at higher heating rates, thus the peak is narrower and should be more intense than those obtained at lower heating rates. In addition, the numerical values can be compared as regard to the T_g values. A general increase in E_a is admitted with the increase in T_g, nevertheless attention must be paid to the dominant crystallization mechanism. In the case of the metaphosphate composition the activation energy is lower than that of the pyrophosphate (127 kJ.mol^{-1} and 140 kJ.mol^{-1} respectively) but the glass transition is higher (313°C and 274°C, respectively). This is due to crystallization which occurs in volume in the case of $Sn_2P_2O_7$ and from surface for $LiPO_3$. Indeed, close to or on interfaces, both thermodynamic and kinetic barriers for nucleation are typically lower than those of bulk values, lowering the activation energy and causing a pre-dominance of surface nucleation [33].

Adiabatic nucleation

From an experimental point of view, the determination of the maximum nucleation temperature only requires to get values of heat of fusion, melting point and the average specific heat at the melting temperature. On the contrary, for the determination of T_{max}, the use of the classical nucleation theory imposes, among other parameters, to know the viscosity-temperature curve and the thermodynamic driving force, which are subjected to more errors. Nevertheless, the remaining question is how well the adiabatic theory can predict T_{max}. An attempt to answer to this question has been carried out [22]. In this previous

work, the calculation of the T_{max}/T_m values have been achieved using both classical and adiabatic nucleation theories, and a comparison with experimental data available has been performed. Two types of glasses were considered, the first one which present internal nucleation and the second one for which internal nucleation was not observed. Taking into account the different approximations of both theories and the uncertainties in the experimental parameters, it has been concluded that the T_{max}/T_m values were in a good agreement. Moreover, a general trend has been settled, glasses which crystallize internally present $T_{max} > T_g$ and $T_g/T_m < 0.58$, on the contrary, for glasses crystallizing only from the surface $T_{max} < T_g$ and $T_g/T_m > 0.58$. Considering the studied phosphate glasses, the metaphosphate and the orthophosphate are clearly obeying to this empirical rule, as displayed in Fig.9. The case of the pyrophosphate is more ambiguous because T_{max} # T_g ($T_{max}/T_g = 0.993$) and there is a clear experimental evidence for this glass to crystallize both from surface and volume. In this specific case, we assume that nucleation occurs in a reasonable period of time, compared to the time scale laboratory and with a short induction time. This limiting case has been also pointed out for the $CaSiO_3$ glass composition [20, 22]. Nevertheless, with a T_g/T_m value of 0.613 and according to [22], $Sn_2P_2O_7$ crystallization should occur only from surface. Consequently, one should consider that the relationship between T_g/T_m and the dominant nucleation mechanism is related to the structure and relaxation kinetics of the supercooled liquid, but it has to be improved.

6. Conclusion

This work was an attempt to obtain information about the crystallization behavior of several phosphate glasses belonging, as much as possible, to the broadest chemical compositions in terms of polymerization. For this purpose, we used several methodologies to precise the dominant crystallization mechanism, to determine the kinetic parameters of the overall crystallization process and finally we tested how well the adiabatic theory was able to predict

the temperature of the maximum nucleation rate. As attested by DSC analysis and SEM observation, performed both on powder and bulk samples, the metaphosphate (Q^2 units) clearly crystallizes from surface, whereas the orthophosphate (Q^0 units) crystallizes in the whole volume. The case of the pyrophosphate (Q^1 units) is a little bit more ambiguous, crystallization occurs first at the surface of the bulk sample but is quickly propagated to the whole volume. This is conceivable by considering that the nucleation time lag is short enough and promotes volume nucleation at the laboratory time scale. All these conclusions are supported by the adiabatic analysis, if there is no doubt concerning the respective behaviors of the metaphosphate and orthophosphate compositions, the same ambiguity is pointed out in the case of the pyrophosphate. Nevertheless, we must keep in mind that the adiabatic model is much less pretentious than the classical nucleation theory because it does not predict quantitative nucleation frequencies. It just give information whether homogeneous or heterogeneous nucleation occurs.

References

[1] J.R. Jones, A.G. Clare: Bio-Glasses: An Introduction (John Wiley & Sons, United Kingdom 2012)

[2] J.H. Campbell, J.S. Hayden, A. Marker: High Power Solid-State Lasers: a Laser Glass Perspective, Int. J. App. Glass Sci. 2 [1], 3-29 (2011)

[3] I. Ahmed, A.J. Parsons, G. Palmer, J.C. Knowles, G.S. Walker, C.D. Rudd: Weight loss, ion release and initial mechanical properties of a binary calcium phosphate glass fibre/PCL composite, Acta Biomaterialia 4, 1307-1314 (2008)

[4] R. Morena: Phosphate glasses as alternatives to Pb-based sealing frits, J. Non-Cryst. Solids 263&264, 382-387 (2000)

[5] X. Yu, J.B. Bates, G.E. Jellison Jr., F.X. Hart: A Stable Thin-Film Lithium Electrolyte: Lithium Phosphorus Oxynitride, J. Electrochem. Soc. 144 [2], 524-532 (1997)

[6] X. Xu, Z. Wen, Z. Gu, X. Xu, Z. Lin: Lithium ion conductive glass-ceramics in the system $Li_{1.4}Al_{0.4}(Ge_{1-x}Ti_x)_{1.6}(PO_4)_3$ (x=0-1.0), Solid State Ionics 171, 207-213 (2004)

[7] S.T. Reis, M. Karabulut, D.E. Day: Structural features and properties of lead-iron-phosphate nuclear wasteforms, J. Nucl. Mat. 304, 87-95 (2002)

[8] R.K. Brow, Review: the structure of simple phosphate glasses, J. Non-Cryst. Solids 263&264, 1-28 (2000)

[9] J. Rocherullé, F. Bourdin, P. Bénard-Rocherullé: The glass to NZP crystal transformation in a mixed alkali germano-phosphate glass matrix, Mater. Res. Bull. 41, 1249–1258 (2006)

[10] T. Kasuga: Bioactive ceramics prepared by sintering and crystallization of calcium phosphate invert glasses. Biomaterials, 20 (15), 1415-1420 (1999)

[11] Y. Zhang: Microstructural characterization and in vitro apatite formation in CaO–P2O5–TiO2–MgO–Na2O glass-ceramics. J. of the Eur. Ceram. Soc., 21 (2), 169 (2001)

[12] T. Kasuga Machinable calcium pyrophosphate glass-ceramics, J. of Mater. Res., 16 (3), 876-880 (2001)

[13] T. Kasuga, T. Kimata, A. Obata: Preparation of a calcium titanium phosphate glass-ceramic with improved chemical durability, J. of the Amer. Ceram. Soc., 92 (8), 1709-1712 (2009)

[14] X. Xu, Z. Wen, Z. Gu, X. Xu, Z. Lin: Lithium ion conductive glass-ceramics in the system $Li_{1.4}Al_{0.4}(Ge_{1-x}Ti_x)_{1.6}(PO_4)_3$ (x=0-1.0), Solid State Ionics 171, 207-213 (2004)

[15] S. Hasegawa, N. Imanishi, T. Zhang, J. Xie, A. Hirano, Y. Takeda, O. Yamamoto: Study on lithium/air secondary batteries-Stability of NASICON-type lithium ion conducting glass-ceramics with water, J. Power Sources 189, 371-377 (2009)

[16] H. Hosono, Z. Zhang, V. Abe: Porous Glass-Ceramic in the Ca0-Ti02-P205 System, J. Am. Ceram. Soc., 72 [9] 1587-90 (1989)

[17] J. Massera, M. Mayran, J. Rocherullé, L. Hupa: Crystallization behavior of phosphate glasses and its impact on the glasses' bioactivity, J. Mater. Sci. 50 3091–3102 (2015)

[18] C.S. Ray, D.E. Day, Determining the nucleation rate curve for lithium disilicate glass by differential thermal analysis, J. Am. Ceram. Soc. 73 439-442 (1990)

[19] H. Yinnon, D.R. Uhlmann, Applications of thermoanalytical techniques to the study of crystallization kinetics in glass-forming liquids, part I: Theory, J. of Non-Cryst. Solids 54 253-275 (1983)

[20] E. Meyer, Adiabatic nucleation, J. Cryst. Growth 74 425-438 (1986)

[21] C. S. Ray, X. Fang, D.E. Day, New Method for Determining the Nucleation and Crystal-Growth rates in Glasses, J. Am. Ceram. Soc. 83 865-872 (2000)

[22] E. D. Zanotto, Isothermal and adiabatic nucleation in glass. J. of Non-Cryst. Solids, 89 361-370 (1987)

[23] R.C. Tolman, the Effect of Droplet Size on SurfaceTension, J. of Chem. Phys. 17 3 333-337 (1949)

[24] V.M. Fokin, A.S. Abyzov, J.W.P. Schmelzer, E.D. Zanotto, Stress induced pore formation and phase selection in a crystallizing stretched glass, J. of Non-Cryst. Solids 356 1679-1688 (2010)

[25] V.V. Chernaya, A.S. Mitiatev, P.S. Chizhov, E.V. Dikarev, R.V. Shpanchenko, E.V. Antipov, M.V. Korolenko, P.B. Fabritchnyi, Synthesis and Investigation of Tin(II) Pyrophosphate $Sn_2P_2O_7$, Chem. Mater. 17 2 284-290 (2005)

[26] S. Inaba, S. Oda, K. Morinaga, Heat capacity of oxide glasses measured by AC calorimetry. J. of Non-Cryst. Solids, 306 42-49 (2002)

[27] W.D. Kingery, H.K. Bowen, D.R. Uhlmann, Introduction to Ceramics, 2nd Ed., John Wiley, Singapore, p. 589 (1991)

[28] J. Rocherullé, S. Chenu, P. Bénard-Rocherullé, Macroscopic and micro-structural aspects of the lithium metaphosphate glass crystallization, J. of Non-Cryst. Solids, 356 2969–2976 (2010)

[29] V.M. Fokin, A.A. Cabral, R.M.C.V. Reis, M.L.F. Nascimento, E.D. Zanotto, Critical assessment of DTA–DSC methods for the study of nucleation kinetics in glasses, J of Non-Cryst Solids, 356 358–367 (2010)

[30] M.C. Weinberg, Interpretation of DTA Experiments Used for Crystal Nucleation Rate Determinations, J. Am. Ceram. Soc. 74 [8] 1905-909 (1991)

[31] P.F. James, Glass ceramics: new compositions and uses, J. of Non Cryst. Solids, 181 1-15 (1995)

[32] H. Kun, W. Yanhan, Z. Chengkui, Z. Huifeng, L. Yonghua, C. Jiang, H. Bin, M. Juanrong, Influence of Al_2O_3 additions on crystallization mechanism and conductivity of Li_2O-GeO_2-P_2O_5 glass-ceramics, Physica B, 406 3947-3950 (2011)

[33] E. D. Zanotto, V. M. Fokin, Recent studies of internal and surface nucleation in silicate glasses, Phil. Trans. R. Soc. Lond. A 361, 591–613 (2003)